

May 20, 2019
BI-TP 2001/14

Spectrum of the Dirac Operator coupled to two-dimensional quantum gravity

L. Bogacz^{1,2}, Z. Burda^{1,2}, C. Petersen¹ and B. Petersson¹

¹Fakultät für Physik, Universität Bielefeld
P.O.Box 100131, D-33501 Bielefeld, Germany

²Institute of Physics, Jagellonian University
ul. Reymonta 4, 30-059 Krakow, Poland

Abstract

We implement fermions on dynamical random triangulation and determine numerically the spectrum of the Dirac–Wilson operator \mathcal{D} for the system of Majorana fermions coupled to two-dimensional Euclidean quantum gravity. We study the dependence of the spectrum of the operator $\epsilon\mathcal{D}$ on the hopping parameter. Using finite size analysis we determine critical exponents controlling the scaling of the lowest eigenvalue of the spectrum including the Hausdorff dimension d_H and the exponent κ which tells us how fast the pseudo-critical value of the hopping parameter approaches its infinite volume limit.

Introduction

Dynamical triangulation approach to quantum gravity has proven to be a very powerful method [1, 2, 3]. In two-dimensions it yields the same results for critical exponents as the Liouville theory [4, 5, 6]. Contrary to the latter, this approach can be straightforwardly generalized to higher dimensional case – simplicial gravity [7, 8]. Results from numerical studies of pure gravity without matter fields in four dimensions showed that the continuum limit of this model does not exist [9]. In order to obtain more realistic models, one has tried to include matter fields and to couple them to gravity [10]. This program has so far succeeded only for bosonic matter. Putting fermions on random simplicial manifold is a more difficult task. In general it requires introducing an additional field of local frames and defining a spin structure

[11, 12, 13]. In the case of a compact manifold this is a topological problem. Although many ingredients of the construction are known and can be generalized to any number of dimensions, the topological part of the problem has been solved so far only in two dimensions [13].

In this paper we will study properties of the Dirac–Wilson operator on two-dimensional dynamical triangulation with spherical topology. We cross-check some properties of the spectrum using the equivalence of the fermionic model with the Ising model on dynamical triangulation, the latter of which is analytically solvable [14, 15, 16].

The paper is organized as follows : First we define the model, then we recall some facts about its relation to the Ising model [12], we present results of numerical studies and shortly conclude at the end by summarizing and listing open questions. In the appendix, for comparison, we calculate the spectrum of the Dirac–Wilson operator on a regular triangulation.

The model

The model of fermions minimally coupled to Euclidean gravity is given by the partition function

$$\mathcal{Z} = \sum_{T \in \mathcal{T}} \mathcal{Z}_T = \sum_{T \in \mathcal{T}} \int \prod_i d\bar{\Psi}_i d\Psi_i e^{-S_T} \quad (1)$$

where the sum goes over d -dimensional simplicial manifolds from a class \mathcal{T} , say, for instance, with spherical topology. Each triangulation is dressed with the fermion field located in the centers of d -simplices. The integral over field on a given triangulation defines the partition function \mathcal{Z}_T , which at the same time provides a weight of this triangulation T in the ensemble. The action reads

$$S_T = -K \sum_{\langle ij \rangle} \bar{\Psi}_i \mathcal{H}_{ij} \Psi_j + \frac{1}{2} \sum_i \bar{\Psi}_i \Psi_i = \sum_{i,j} \bar{\Psi}_i \mathcal{D}_{ij} \Psi_j, \quad (2)$$

where the sum over $\langle ij \rangle$ runs over all oriented links of the triangulation T . The hopping operator is written as

$$\mathcal{H}_{ij} = \frac{1}{2} (1 + n_{ij}^{(i)} \cdot \gamma) \mathcal{U}_{ij}. \quad (3)$$

The Dirac–Wilson operator is denoted by \mathcal{D}_{ij} and the spin connection by \mathcal{U}_{ij} . In order to be able to calculate spinor and vector components, we endow each d -simplex with an orthonormal local frame. A frame is a set of orthonormal

oriented vectors e_a , $a = 1, \dots, d$. To each vector e_a we ascribe a Dirac gamma matrix γ^a , in such a way that its numerical value is identical in each frame. The local vector n_{ij} in eq. (3) is a unit vector which points from the center of the simplex j to the center of one of its neighbors i . It just tells us the direction of local derivative. The inner product of this vector and of gamma matrices, which denoted by dot in (3), has to be understood as a sum of gamma matrices γ^a multiplied by the components of $[n_{ij}^{(i)}]_a$ in the given frame at i , denoted by the upper index. Thus, the product of the same vector n_{ij} expressed in another frame yields a different matrix : $n_{ij}^{(j)} \cdot \gamma = [n_{ij}^{(j)}]_a \gamma^a$.

As mentioned the matrix \mathcal{U}_{ij} plays the role of spin connection. It allows us to parallel transport a spinor from the simplex j to the simplex i , or in other words, to recalculate spinor components between two neighboring frames i and j . The matrix \mathcal{U}_{ij} is an image in the spinorial representation of the rotation matrix U_{ij} which parallel transports vectors. The map $U_{ij} \rightarrow \mathcal{U}_{ij}$ is not unique in that it is defined only up to sign. As we will see below, the signs of \mathcal{U} must be adjusted to fulfill a consistency condition (8) for all elementary plaquettes of the simplicial manifold. This is a topological problem.

This problem has been solved in two-dimensions where an explicit construction of the signs of the spin connection matrices \mathcal{U}_{ij} has been given [13]. Let us shortly recall the main steps of the construction.

In two dimensions each orthonormal frame consists of two vectors e_{ia} where a is 1 or 2. The first index of e_{ia} refers to the triangle in which the frame is located. For any pair of neighboring triangles i, j we can define a spin connection as a two by two rotation matrix $[U_{ij}]_b^a$, such that¹ $e_{ia} = \sum_b [U_{ij}]_b^a e_{jb}$. Using matrix notation this relation can be written as $e_i = U_{ij} e_j$, where

$$U_{ij} = e^{\epsilon \Delta \phi_{ij}} = \begin{pmatrix} \cos \Delta \phi_{ij} & \sin \Delta \phi_{ij} \\ -\sin \Delta \phi_{ij} & \cos \Delta \phi_{ij} \end{pmatrix} \quad (4)$$

and $\Delta \phi_{ij}$ is the relative angle between the two neighboring frames. ϵ is the standard antisymmetric tensor.

The trace of an elementary loop around a dual plaquette is a geometrical invariant directly related to the curvature (deficit angle) of the vertex in the center of the plaquette. One can check that

$$\frac{1}{2} \text{Tr} U U \dots U = \frac{1}{2} \text{Tr} e^{\epsilon(2\pi - \Delta_P)} = \cos \Delta_P, \quad (5)$$

where Δ_P is the deficit angle of the vertex in middle of the plaquette. The product $U U \dots U$ of connections on all links on the plaquette perimeter P

¹In general a connection can be a dynamical field.

is a rotation matrix which gives the integrated rotation of a tangent vector parallel transported around this loop. The equation (5) is a sort of Wilson discretization [17, 18] of curvature calculated from the Cartan structure equations [19].

Now the idea is to write down an analogous equation as (5) in the spinorial representation. First we have to introduce a parallel transporter \mathcal{U}_{ij} for spinors for each pair of neighboring vertices. This is exactly the object which we need in (3). The connection \mathcal{U}_{ij} is an spinorial image of U_{ij} . One can choose a representation of gamma matrices such that $U_{ij} = \mathcal{U}_{ij}^2$. One immediately sees that indeed \mathcal{U}_{ij} can be calculated for a given U_{ij} up to sign. When defining the Dirac–Wilson operator (3) we cannot allow for ambiguities, so we have to give a unique prescription how to calculate \mathcal{U}_{ij} . We do this by choosing

$$\mathcal{U}_{ij} = e^{\frac{\epsilon \Delta \phi_{ij}}{2}} = \begin{pmatrix} \cos \frac{\Delta \phi_{ij}}{2} & \sin \frac{\Delta \phi_{ij}}{2} \\ -\sin \frac{\Delta \phi_{ij}}{2} & \cos \frac{\Delta \phi_{ij}}{2} \end{pmatrix} \quad (6)$$

and specifying the angles $\Delta \phi_{ij}$ without the $2n\pi$ freedom. More precisely we define $\Delta \phi_{ij} = \phi_i^{(j)} - \phi_j^{(i)} + \pi$ where the angle $\phi_i^{(j)}$ at triangle j is the angle between the vector e_{j1} of the frame at j and the vector n_{ij} (pointing from j to i), and likewise $\phi_j^{(i)}$ at triangle i is the angle between the vector e_{i1} and the vector n_{ji} (pointing from i to j) (see fig.1). Both the angles are restricted to the range $[0, 2\pi)$ and both are measured in the same direction, say clockwise. Thus the angle $\Delta \phi_{ij}$ is defined without the 2π ambiguity and hence the rotation matrix \mathcal{U}_{ij} is also uniquely determined including the total sign.

One can easily check that, for the definition (6) of \mathcal{U}_{ij} 's, the parallel transporter around an elementary loop gives

$$\frac{1}{2} \text{Tr} \mathcal{U} \mathcal{U} \dots \mathcal{U} = S_P \cos \frac{\Delta_P}{2}. \quad (7)$$

The argument of cosinus got halved $\Delta_P \rightarrow \Delta_P/2$ in comparison with (5) because for each link on P we have $\mathcal{U}^2 = U$. The total sign S_P of the product $\mathcal{U} \mathcal{U} \dots \mathcal{U}$ has to be calculated. It turns out it depends on all angles $\Delta \phi_{ij}$ on the loop and it may admit either value ± 1 [13].

The presence of elementary plaquettes which would have negative sign is an unwanted effect. A spinor transported around a flat plaquette, $\Delta_P = 0$, with $S_P = -1$, would change the sign $\psi \rightarrow -\psi$. We require that the parallel transport around a close loop in a flat patch not change a spinor.

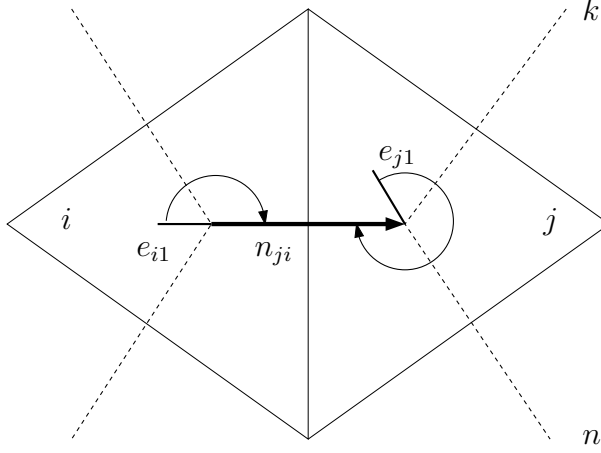


Figure 1: Local geometry of two neighboring triangles is shown. The position of the first frame vector e_1 for a given triangle is marked by a line emerging from the triangle center. The position of the second frame vector e_2 is implicitly given by the fact that the angle between e_1 and e_2 counted clockwise is $\pi/2$. The vector n_{ij} points between the neighboring centers. The arch in the triangle i represents the angle $\phi_j^{(i)}$ between e_{i1} and n_{ij} ; and the arch in the triangle j – the angle $\phi_i^{(j)}$ between e_{j1} and n_{ji} . In the example shown in figure $\phi_j^{(i)} = \pi$, $\phi_i^{(j)} = 5\pi/3$, and for other two neighbors of j : $\phi_k^{(j)} = \pi/3$, $\phi_n^{(j)} = \pi$.

Furthermore, we require positivity of the sign $S_P = +1$ for all elementary plaquettes

$$S_P = +1, \quad \forall P. \quad (8)$$

One can give the following argument in favor of the sign positivity of each elementary loop. An elementary loop goes through triangles sharing a vertex. Geometry of a patch consisting of those triangles corresponds to geometry of a cone. It is everywhere flat except the vertex where it is singular. One can regularize such geometry by smoothing the peak of the cone (making it differentiable) in a very small region with radius $\epsilon \approx 0$. Such a regularization does not affect the loop which lies in a distance $R \gg \epsilon$ from the vertex. Continuously shrinking the loop in such a regularized geometry, one can continuously change the angle of the loop rotation matrix without changing the sign. A completely shrunken loop must have positive sign since it lies in a flat patch. This implies $S_P = +1$. One can also check that the consistency condition (8) plays an essential role in the topological considerations or in deriving the equivalence with the Ising model.

The construction of the connections given in (6) does not fulfill the consistency condition (8). We will therefore modify the construction of \mathcal{U} 's by introducing for each link an additional sign degree of freedom s_{ij}

$$\mathcal{U}_{ij} = s_{ij} e^{\frac{\epsilon \Delta \phi_{ij}}{2}}. \quad (9)$$

One can show that this freedom is sufficient to globally, for each elementary loop, fulfill the consistency condition (8), on a triangulation of an orientable manifold. Thus, technically, to define the Dirac–Wilson operator on a triangulation, we have to first assign an orthonormal frame to each triangle, and then for the frame assignment, to find link signs s_{ij} meeting the consistency condition (8) for each plaquette. The remaining part is straightforward. Namely, we express the operator \mathcal{U}_{ij} in terms of the angles $\phi_i^{(j)}$ and $\phi_j^{(i)}$ and likewise, the product $n_{ij}^{(i)} \cdot \gamma$ in terms of $\phi_j^{(i)}$. Thus, we parameterize the hopping operator \mathcal{H}_{ij} entirely by $\phi_i^{(j)}$ and $\phi_j^{(i)}$ and s_{ij} . For each pair of neighboring triangles the angles can be read off from the given frame assignment (see fig.1).

Choosing the following representation of gamma matrices : $\gamma_1 = \sigma_3$, $\gamma_2 = \sigma_1$, where the σ are Pauli matrices. We eventually arrive at

$$\mathcal{H}_{ij} = s_{ij} \cdot \begin{pmatrix} \sin \frac{\phi_j^{(i)}}{2} \cos \frac{\phi_i^{(j)}}{2} & \sin \frac{\phi_j^{(i)}}{2} \sin \frac{\phi_i^{(j)}}{2} \\ -\cos \frac{\phi_j^{(i)}}{2} \cos \frac{\phi_i^{(j)}}{2} & -\cos \frac{\phi_j^{(i)}}{2} \sin \frac{\phi_i^{(j)}}{2} \end{pmatrix}. \quad (10)$$

We see that in two dimensions the Dirac–Wilson operator on a triangulation T is given by a matrix consisting of two-by-two blocks

$$[\mathcal{D}_{ij}]_{\alpha}^{\beta} = \begin{cases} -K [\mathcal{H}_{ij}]_{\alpha}^{\beta} & \text{if } i, j \text{ are neighbors on } T, \\ \frac{1}{2} \delta_{\alpha}^{\beta} & \text{if } i = j, \\ 0 & \text{otherwise.} \end{cases} \quad (11)$$

The blocks \mathcal{H}_{ij} have a very simple structure. In fact, we can simplify it further by restricting the set of values of the angles in (10) from the whole interval $[0, 2\pi)$ to a discrete set of three values separated by $2\pi/3$, for instance, $\pi/3, \pi, 5\pi/3$. For this choice, the first vector e_1 of a frame at a triangle points from the center of the triangle to one of its vertices. In a sense, this set of three frame positions is a minimal set reflecting the symmetry of equilateral triangle.

Since physical quantities do not depend on the choice of frames, this restriction is a sort of gauge condition. With this choice, the blocks (10) may admit only nine different forms. They can be precomputed. For example, for the frame assignment as in fig.1 $\phi_i^{(j)} = 5\pi/3$, $\phi_j^{(i)} = \pi$ and for $s_{ij} = 1$ we have

$$\mathcal{H}_{ij} = \begin{pmatrix} -\frac{\sqrt{3}}{2} & \frac{1}{2} \\ 0 & 0 \end{pmatrix} \quad , \quad \mathcal{H}_{ji} = \begin{pmatrix} 0 & -\frac{1}{2} \\ 0 & -\frac{\sqrt{3}}{2} \end{pmatrix} . \quad (12)$$

Fermions and the Ising model

The idea is now to calculate spectra of the Dirac–Wilson operator for different triangulations from the ensemble (1). Summing up (averaging) all the spectra we obtain the spectrum of the Dirac–Wilson operator for fermions interacting with 2d gravity. More precisely, we will consider a field of Majorana-fermions coupled to gravity. At the critical point it corresponds to the conformal field with the central charge $c = 1/2$.

Denote the components of the spinor Ψ by Ψ_α , and of $\bar{\Psi}$ by Ψ^β . The Majorana condition reads : $\Psi^\beta = \epsilon^{\beta\alpha}\Psi_\alpha$ or $\Psi_\alpha = \Psi^\beta\epsilon_{\beta\alpha}$, where ϵ is the standard antisymmetric tensor, In this notation, the action for Majorana fermions can be written as

$$S_T = \sum_{ij} \Psi_i^\alpha [\mathcal{D}_{ij}]_\alpha^\beta \Psi_{j\beta} = \sum_{ij} \Psi_{i\alpha} \widehat{\mathcal{D}}_{ij}^{\alpha\beta} \Psi_{j\beta} , \quad (13)$$

where

$$\widehat{\mathcal{D}}_{ij}^{\alpha\beta} = \epsilon^{\alpha\gamma} [\mathcal{D}_{ij}]_\gamma^\beta , \quad (14)$$

or in short $\widehat{\mathcal{D}} = \epsilon \mathcal{D}$. One can show that $\widehat{\mathcal{D}}$ is antisymmetric under the change of pairs of indices

$$\widehat{\mathcal{D}}_{ij}^{\alpha\beta} = -\widehat{\mathcal{D}}_{ji}^{\beta\alpha} , \quad (15)$$

and hence $\text{Pf}^2 \widehat{\mathcal{D}} = \text{Det} \widehat{\mathcal{D}} = \text{Det} \mathcal{D}$. For each triangulation individually, the integral over fermions in (1) yields Pfaffian of the matrix $\widehat{\mathcal{D}}$. Thus for Majorana fermions on a two-dimensional triangulation the partition function (1) is a sum of Pfaffians of the Dirac–Wilson operator

$$\mathcal{Z} = \sum_{T \in \mathcal{T}} \mathcal{Z}_T = \sum_{T \in \mathcal{T}} \text{Pf} \widehat{\mathcal{D}}_T = \sum_{T \in \mathcal{T}} \text{Det}^{1/2} \mathcal{D}_T . \quad (16)$$

In the last step we have used the inequality $\text{Pf } \mathcal{D}_T > 0$, which can be proven by the hopping parameter expansion. The consistency condition (8) turns out to be essential in the proof. Namely, one shows that the Pfaffian is represented as a sum over loop configurations each of which contributes a positive factor if the condition (8) is met [13].

Using this expansion one can also establish the equivalence between the partition \mathcal{Z}_T with the partition function of the nearest neighbor Ising model with spins σ_{i_*} located at the vertices i_* of T

$$Z_T = \sum_{\{\sigma_*\}_T} e^{-\beta E_T} \quad (17)$$

where

$$E_T = - \sum_{(i_*, j_*) \in T} (\sigma_{i_*} \sigma_{j_*} - 1). \quad (18)$$

The partition functions Z_T (17) and \mathcal{Z}_T (1) are equal for

$$K = \frac{e^{-2\beta}}{\sqrt{3}}. \quad (19)$$

In the derivation of this equivalence one identifies loop configurations, arising in the hopping expansion of \mathcal{Z}_T with domain walls of the Ising model. Again, the consistency condition (8) plays the crucial role here. For a non-spherical triangulation one has to carefully treat topological effects related to the existence of non-contractable loops which may give a negative contribution for antiperiodic boundary conditions. One can get rid of all negative contributions performing the GSO projection that is summing over all spin structures of the manifold [20]. This and another topological issues will be discussed elsewhere. Here we will restrict ourselves to spherical triangulations for which we automatically have $\mathcal{Z}_T = Z_T$ for each triangulation $T \in \mathcal{T}$ and hence also for the sum over all triangulations in \mathcal{T}

$$\mathcal{Z} = Z \equiv \sum_{T \in \mathcal{T}} Z_T. \quad (20)$$

The critical temperature of the Ising model for the partition function Z is known analytically $\beta = \frac{1}{2} \ln \frac{131}{85} \approx 0.2162730$ [16]. Translating the critical temperature to the hopping parameter (19) we obtain the following critical value

$$K_{cr} = \frac{85\sqrt{3}}{393} \approx 0.3746166 \quad (21)$$

for which fermions become massless. Another interesting point which can be deduced from the equation (19) is that $K_{max} = 1/\sqrt{3}$ corresponds to $\beta = 0$ which is the border $\beta = 0$ between the ferromagnetic and antiferromagnetic regimes. For $\beta < 0$ one expects frustration in the Ising model on a triangulation and hence that the lowest energy state is highly degenerated. As we will see below, the spectrum of the Dirac-Wilson operator is insensitive to passing over this border. In our considerations we will, however, restrict K to be in the range $[0, K_{max}]$.

The equivalence of the partition functions Z_T and \mathcal{Z}_T may be used to relate the average energy \bar{E}_T of the Ising model on a triangulation T to eigenvalues of the Dirac-Wilson operator. Differentiating both sides of (16) with respect to β we obtain

$$\bar{e}_T = \frac{\bar{E}_T}{N} = -\frac{1}{N} \frac{\partial}{\partial \beta} \ln Z_T = 1 - \frac{\sum_a \lambda_a^{-1}}{2N}, \quad (22)$$

where λ_a are eigenvalues of the Dirac-Wilson operator \mathcal{D}_T . For our choice of the representation of gamma matrices, \mathcal{D}_T is a real matrix. Its spectrum consists of either real eigenvalues or of pairs of complex conjugates. Thus the sum on the right hand side of (22) is a real number. Similarly, the fluctuations of the Ising energy on the triangulation T are given by

$$\sigma_T^2 = \frac{\bar{E}_T^2 - \bar{E}_T^2}{N} = \frac{1}{N} \frac{\partial^2}{\partial \beta^2} \ln Z_T = -\frac{\sum_a \lambda_a^{-2}}{2N} + \frac{\sum_a \lambda_a^{-1}}{N}. \quad (23)$$

Averaging over triangulations we obtain the energy density and heat-capacity of the Ising model coupled to gravity calculated in terms of the eigenvalues of the Dirac-Wilson operator

$$e = \langle \bar{e}_T \rangle = 1 - \left\langle \frac{1}{2N} \sum_a \lambda_a^{-1} \right\rangle, \quad (24)$$

$$c_v = \beta^2 \langle \sigma_T^2 \rangle = \beta^2 \left\{ -\left\langle \frac{1}{2N} \sum_a \lambda_a^{-2} \right\rangle + \left\langle \frac{1}{N} \sum_a \lambda_a^{-1} \right\rangle \right\}. \quad (25)$$

The equivalence of the models can also be very useful in MC simulations of the model. To show this, let us compare three numerical experiments in which (a) the Ising model is used to generate triangulations and to measure the Ising energy and heat capacity; (b) the Ising model is used as a generator of triangulations but measurements are carried out using the fermion dressing; (c) the fermionic model is used both to generate triangulations

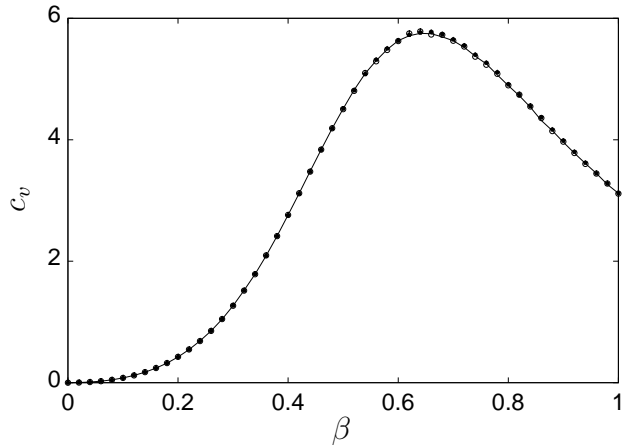


Figure 2: Heat capacity $c_v(\beta)$ for the system with $N = 16$ triangles for the three cases discussed in the text : (a) ising-ising (line); (b) ising-fermion (filled symbols); (c) fermion-fermion (empty symbols). The three methods give the same results within the error bars, which are here of order of the size of the symbols used.

and to perform measurements. As shown in fig.2 the three methods yield exactly the same results. The methods differ, however, significantly in the CPU time needed to generate results of the same quality. The first difference comes from the configuration generator which is much faster for the Ising model than for the fermionic determinant. In the latter case, to calculate a Metropolis weight for a single local change of triangulation, *i.e.* a flip of one link on the triangulation, requires the recomputation of the determinant of the Dirac–Wilson operator on the modified lattice. This is a tedious task for which the number of operations grows with the third power of the system size N . Thus one expects that the time of a sweep through the lattice grows as N^4 for the fermionic configurations generator. One sweep for the Ising model, which consists of a sweep of local updates of Ising spins, a fixed number of Wolff cluster updates, and a sweep of local changes of triangulation, lasts in CPU units roughly proportionally to the system size N . Thus, only for very small lattices the fermionic algorithm is competitive with the Ising generator of triangulations. As far as measurements are concerned the situation is more complex. For example, one cannot determine the spectrum of the Dirac–Wilson operator using only the Ising dressing. One can, however, do the opposite. For a given lattice, the time of calculating all eigenvalues of the Dirac–Wilson operator is proportional to N^3 . Having done this, one is able for this triangulation to exactly calculate the Ising energy (22) and

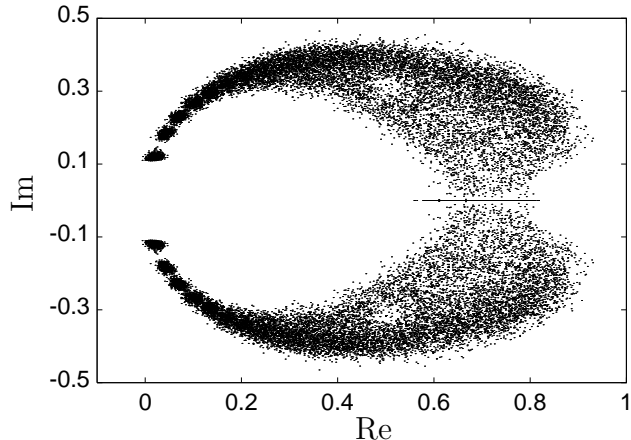


Figure 3: The distribution of eigenvalues λ of the Dirac–Wilson operator for $N = 64$ and $K = 0.364$ on random lattice.

it higher moments (23) without statistical fluctuations. If one instead used the Ising model, one has to sample Ising configuration many times to reduce the error. In general, the cost of a single measurement of the energy is proportional to N . The error of the single measurement of the energy density decreases like $1/\sqrt{N}$. Summarizing, we expect the CPU time to measure energy with a given precision to grow as \sqrt{N} . The CPU time grows rapidly with the order for measurements of higher moments of energy.

In order to obtain the data the quality presented in fig. 2 for $N = 16$, the methods discussed above required (a) 1000 CPU min. (b) 6 CPU min. and (c) 100 min. on the computer Alpha XP1000/EV6/500 MHz.

Spectrum of the Dirac–Wilson operator

In the production runs we use the method (b) which relies on generating triangulations from the partition function of the Ising model. At each measurement we ignore the Ising dressing and we assign frames e_i and s_{ij} -signs to the triangulation to reconstruct the Dirac–Wilson operator (10).

A typical spectrum of the Dirac–Wilson operator on random triangulation is shown in fig.3. The main effect on the spectrum of changing the hopping parameter K is to rescale it around the point $(\frac{1}{2}, 0)$. The positions of the two claw-shaped ends of the spectrum move with K . One can find a value of K for which the ends lie closest from the origin $(0, 0)$. This value can be treated as a pseudo-critical value K_* for which the mass of the fermion excitation is minimal. For $K < K_*$ the origin $(0, 0)$ lies outside the claws, while for

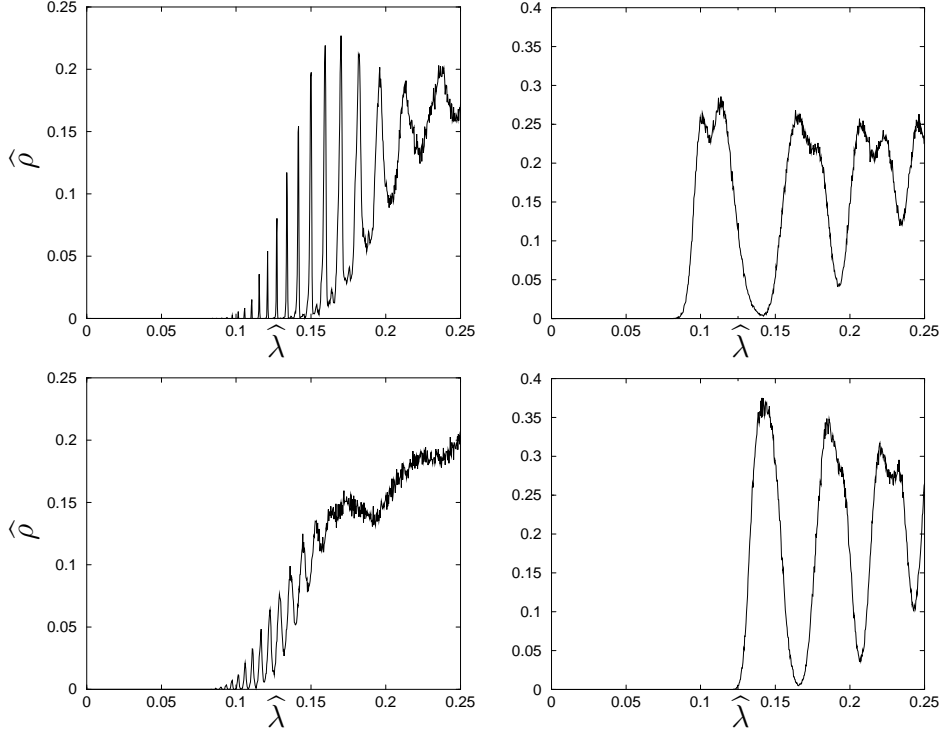


Figure 4: Spectra of the operator $\epsilon\hat{\mathcal{D}}$ for $N = 64$; on the left for $K = 0.522$ (upper) and $K = 0.473$ (lower) – both above the pseudo-critical point $K_* = 0.364$; on the right for $K = 0.350$ (upper) and $K = 0.287$ (lower) – below the pseudo-critical point.

$K > K_*$ inside. In fact, this is the main difference between the two regimes since beside the scaling factor the shape of the spectrum is almost constant. It does not change either when one crosses the limit $K = K_{max}$.

The claws of the pseudo-critical spectra successively close when the size, N , of the system is increased. They eventually close entirely at the origin $(0, 0)$ for infinite N , signaling the occurrence of massless excitations.

As an alternative to spectrum of the operator \mathcal{D} one can study spectrum of the operator $\hat{\mathcal{D}} = \epsilon\mathcal{D}$ which is closer related, in spirit, to Majorana fermions. Since it is purely imaginary, its eigenvalue density is one dimensional, which can be expressed by

$$\hat{\rho}(x) = \lim_{N \rightarrow \infty} \frac{1}{N} \left\langle \sum_{\hat{\lambda}} \delta(x - i\hat{\lambda}) \right\rangle. \quad (26)$$

For finite N it can be approximated by a histogram. We study the depen-

dence of the shape of the histograms on K . We observe that there is a change of regimes when K crosses the pseudo-critical value K_* . For K above K_* , the lowest part of the spectrum exhibits an oscillatory pattern. It gradually shrinks and the oscillation eventually disappears when the K passes from the phase below to the phase above the pseudo-critical value. Typical spectra in the two phases are shown in fig.4. Another interesting feature of the histograms, is the presence of singular peaks for which the number of entries grows with the size of the lattice. The peaks lie outside the range displayed in the figure. We show in the appendix that such peaks are also present in the spectrum on the regular lattice.

Again, a physically important feature of the spectrum is the position of the lowest eigenvalue. The position, at which the spectrum terminates at the low eigenvalue end² moves with K . We study this dependence quantitatively in the following way. Using the Lanczos algorithm³ we determine the distribution of the lowest eigenvalue for a given lattice size N and plot the position of the center of mass of this distribution M as a function of the hopping parameter K . For small K the distribution has a single gaussian shape. When K is increased the shape begins to deviate from the gaussian form. When K approaches K_{max} this distribution consists of many separate peaks and exhibits an oscillatory pattern similar to the one of the upper left spectrum in fig. 4.

The function $M(K)$ which represents the position of the center of mass against K has a minimum (see fig.5). The value of the minimum M_* is a sort of a mass gap. While its position K_* is a pseudo-critical hopping parameter. We determined K_* and M_* for different system sizes. The results are collected in the table 1. We fitted the data points to the following finite size scaling formulas

$$M_* = \frac{b}{N^{\frac{1}{d_H}}} \left(1 + \frac{t}{N} \right) \quad , \quad K_* = K_\infty - \frac{a}{N^\kappa} . \quad (27)$$

² The spectrum is symmetric $\hat{\rho}(\lambda) = \hat{\rho}(-\lambda)$. In the text we consider only its positive part.

³The Lanczos algorithm [21] is an iterative procedure to calculate eigenvalues. It is frequently used to approximately determine the lowest part of the eigenvalue spectra of large matrices, for which exact standard diagonalization algorithms would require a too long time. In a single iteration step the Lanczos algorithm finds one approximated eigenvalue and improves quality of the previously calculated ones. As a rule it first produces the smallest and the largest eigenvalues and then successively fills up the remaining part of the spectrum, The accuracy increases with the number of iterations. We checked in our case using matrices of sizes up to 128, that when we keep the number n of iteration proportional to the size of the matrix $n = cN$ with, $c = 0.25$, the distribution of the lowest eigenvalue agrees with the one obtained by an exact algorithm.

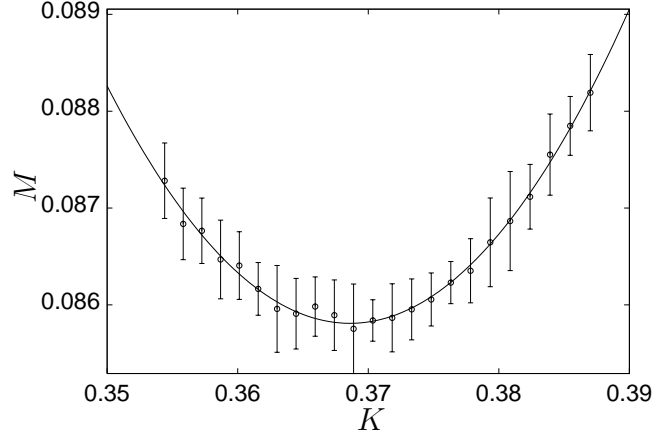


Figure 5: The position of the center of mass is shown for the distribution of the smallest eigenvalue of the operator $\hat{\mathcal{D}}$ for $N = 96$ as a function of the hopping parameter K .

N	K_*	M_*
32	0.352(3)	0.1395(5)
48	0.360(2)	0.1162(4)
64	0.364(2)	0.1016(2)
96	0.368(2)	0.0858(2)
128	0.370(1)	0.0766(2)
192	0.372(2)	0.0656(3)
256	0.372(2)	0.0589(3)
384	0.374(2)	0.0509(3)
512	0.374(2)	0.0459(4)
768	0.375(3)	0.0397(2)
1024	0.375(1)	0.0359(3)

Table 1: Positions and values of the minima of the function $M(K)$ representing the center of mass of the distribution of the smallest eigenvalue of the operator $\hat{\mathcal{D}}$ for different system sizes N .

The exponent d_H is the fractal dimension of the surface given by $L = N^{1/d_H}$, which defines a typical linear extent of the system. When the physical mass is equal zero, L sets the scale for the correlation length. Its inverse gives the minimal eigenvalue of the spectrum M_* . For smaller systems one expects corrections to the scaling. We take it into account by introducing a phenomenological correction t/N to the scaling formula (27). This correction significantly improves quality of the fit for the studied range of volumes. The best fit to the formula is $1/d_H = 0.348(4)$, $b = 0.40(1)$ and $t = 5.7(5)$. The corresponding curve is plotted in fig.6. The curve fits indeed very well to all the data points. The error bars of the best fit parameters were estimated by jack-knife.

We compared the goodness of the best fits to the formula (27) and analogous formulas in which the correction was substituted by $t/N^{1/2}$ and $t/N^{3/2}$. For the formula (27) with the correction t/N we obtain $\chi^2/\text{d.o.f.} = 0.52$ while in the other two cases 1.66 and 1.83, respectively. Among those three the phenomenological form t/N of the correction is the best in this range. We have also checked that the fitted value $1/d_H = 0.348(4)$ is stable against the successive removal of the data points of the smallest volumes.

The calculated Hausdorff dimension $d_H = 2.87(3)$ lies three standard deviations from the theoretical prediction $d_H = 3$ obtained by considerations of a test fermion in the gravitational background coupled to matter field with the central charge $c = 1/2$ [23]. One should take this result with a precaution for the following reasons: First, there are other theoretical predictions for the Hausdorff dimension which suggest that d_H is rather equal four or more [24]. Second, measurements of the Hausdorff are known to have strong finite size corrections. For pure gravity, for example, where calculations are easier, the effective Hausdorff dimension, computed using the distribution of distances between centers of triangles, varies very slowly with the size N [24]: for example when N changes from 250 to 2000, the estimated values grow slowly from 2.715(50) to 2.996(26), and they continue to grow further outside this range. Even for sizes as big as $N = 32000$ the measured value 3.411(89) is smaller than the theoretical prediction which for pure gravity is $d_H = 4$ [22].

The best fit for the second formula in (27) is given by $K_\infty = 0.3756(16)$, $\kappa = 1.03(30)$ and $a = 0.9(5)$ (see fig.7). The limiting value K_∞ is in agreement with the theoretically calculated critical value K_{cr} (21). The scaling exponent κ is almost equal 1 which would suggest a sort of kinematic scaling, related to the fact that the average distance between eigenvalues decreases as $1/N$. For the moment we do not have a strict argument.

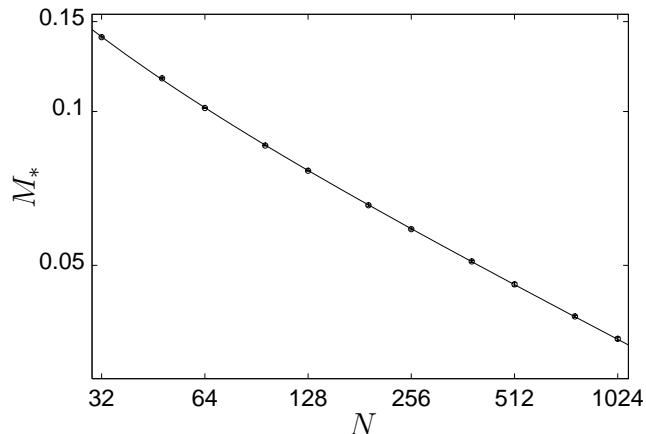


Figure 6: The mass gap M_* for different system sizes N , and the curve representing the best fit to the formula (27) : $1/d_H = 0.348(4)$, $b = 0.40(1)$ and $t = 5.7(5)$.

Discussion

We have discussed the properties of the Dirac–Wilson operator on a random triangulation. In particular we have shown how to extract from the spectrum the information about physical quantities like the fractal dimension or the critical value of the hopping parameter of fermions interacting with gravity at which they become massless.

There are many natural extensions of the studies presented in this work. One should try to understand properties of the spectrum of the Dirac operator from the point of view of the random matrix theory [25, 26, 27]. This is a slightly different type of randomness than the one provided by the coupling to the vector gauge field which is usually studied in the context of QCD. However exactly this type of randomness may be important in quantum gravity.

Next, one can investigate the quenched approximation by considering a model of fermions on random triangulation without the back-reaction of fermions on gravity. Such a model describes a test particle in pure gravity. From this exercise one could perhaps draw a general lesson about the effect of quenching on the spectrum of the Dirac operator. This can be important because this type of approximation is frequently used in many physical contexts, for example, in QCD. However, one usually is not able to quantify the effects of quenching.

Furthermore, one can study effects of changing topology by considering non-spherical 2d-triangulations. As mentioned it requires a careful treatment

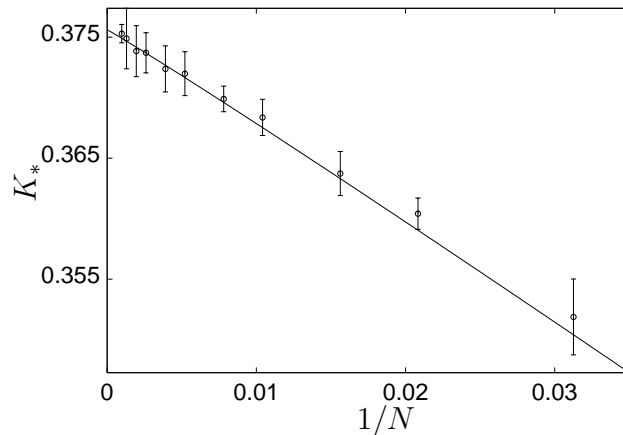


Figure 7: The pseudo-critical parameter K_* for different system sizes N , and the curve representing the best fit to the scaling formula (27) : $K_\infty = 0.3756(16)$, $\kappa = 1.03(30)$ $a = -0.9(5)$, plotted as a function of $1/N$.

of various spin structures which may be admitted by a manifold. Contrary to higher dimensional case, where the existence of spin structure is related to the second Stiefel-Whitney class [19], here the question of the existence reduces to the orientability of the manifold. Also the classification of spin structures is relatively simple in the 2d case. The spin structures can be classified by a set of signs defined on all classes of non-contractable loops. The signs tell us whether boundary conditions for a parallel transport of a spinor around those loops are periodic (+1) or anti-periodic (-1). For a manifold with genus h , there are $2h$ different classes of non-contractable loops and hence there are 2^{2h} different spin structures.

Finally one should try to find a lattice implementation of the Dirac operator for higher dimensional compact simplicial manifolds. Many parts of the construction can be directly generalized from the 2d case; actually almost all, except the link sign degrees of freedom, s_{ij} (9), which as it turns out are not sufficient in general case for the connections \mathcal{U}_{ij} to fulfill the consistency condition for all plaquettes (8).

Acknowledgments

We thank J. Jurkiewicz, A. Krzywicki, E. Laermann, D. E. Miller and J. Tabaczek for many discussions. This work was supported in part by the EC IHP grant HPRN-CT-1999-00161 and by the Polish Government Project (KBN) 2P03B 01917. At the first stage of this work L.B. was supported by

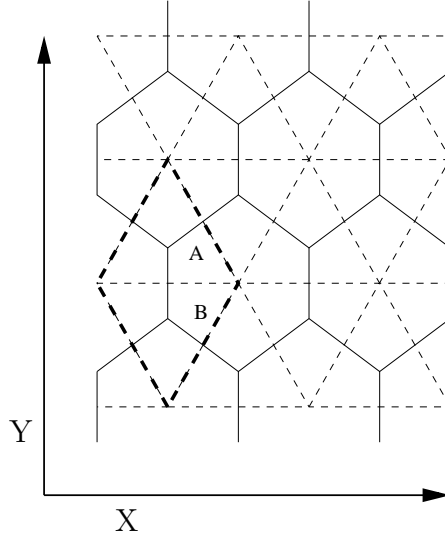


Figure 8: Regular triangulation of the plane and its dual lattice. Fermions live on the vertices of the dual (honey-comb) lattice. The elementary cell contains two distinct dual node positions denoted by A and B .

a DAAD fellowship.

Appendix

For a comparison in the appendix we calculate spectrum of the Dirac–Wilson operator on the regular planar triangulation built of equilateral triangles with fermion field located in the centers of triangles. If one connects the centers by links, they form a dual lattice; in this case it is a honey-comb lattice (see fig.8). It is convenient to divide the vertices of this lattice into two classes A and B forming a check-board. The fundamental cell on the triangulation contains one site of each. One reconstructs the entire triangulation translationally copying the fundamental cell using multiples of two the vectors $d_1 = n_0 + n_1$, and $d_2 = n_0 + n_2$ constructed from the link vectors $n_0 = (0, 1)$, $n_1 = (\sqrt{3}/2, 1/2)$, $n_2 = (-\sqrt{3}/2, 1/2)$.

Using translational symmetry of the lattice we can now rewrite the action

(2) in the following form

$$\begin{aligned}
S = & -\frac{K}{2} \sum_i \sum_{d=1}^2 [\bar{\psi}_{i+d,A}(1 + n_d \cdot \gamma) \psi_{i,B} + \bar{\psi}_{i,B}(1 - n_d \cdot \gamma) \psi_{i+d,A}] \\
& -\frac{K}{2} \sum_i [\bar{\psi}_{i,A}(1 - n_0 \cdot \gamma) \psi_{i,B} + \bar{\psi}_{i,B}(1 + n_0 \cdot \gamma) \psi_{i,A}] \\
& +\frac{1}{2} \sum_i [\bar{\psi}_{i,A} \psi_{i,A} + \bar{\psi}_{i,B} \psi_{i,B}] ,
\end{aligned} \tag{28}$$

where the first index in $\psi_{i,A}$ is a double index consisting of two integers (i_1, i_2) , which give the position of the cell $x = i_1 d_1 + i_2 d_2$, while the second label denotes the position A or B within the cell. In the component notation, the addition of d_1 to i corresponds to $(i_1, i_2) \rightarrow (i_1 + 1, i_2)$, and of d_2 to $(i_1, i_2) \rightarrow (i_1, i_2 + 1)$. In the expression (28) we have used a shorthand notation denoting the sum over d_1 and d_2 by $d = 1, 2$. We can now partially diagonalize the problem using the Fourier transform of the index $i = (i_1, i_2)$ to the momentum space $p = (p_1, p_2)$. This leads us to a block-diagonal matrix consisting of four by four blocks. Each block $D(p)$ corresponds to one Fourier mode $\bar{\psi}_p D(p) \psi_p$. The four by four matrix $D(p)$ is indexed by the spinor index of ψ and of the position label A or B. For each p , diagonalization of $D(p)$ yields four eigenvalues

$$\lambda_p = \frac{1}{2} \pm K \frac{\sqrt{3}}{2} \sqrt{w \pm i \sqrt{4 - (w - 1)^2}}, \tag{29}$$

where

$$w = \cos(p_1) + \cos(p_2) + \cos(p_1 - p_2). \tag{30}$$

The distribution of eigenvalues (29) on a finite lattice $L \times L$ with periodic boundary condition in the $d_{1,2}$ directions is shown in fig.9. In this case the momenta admit the values $p_{1,2} = 2\pi k_{1,2}/L$, where $k_{1,2} = 0, \dots, L - 1$ and hence the operator has $4L^2$ eigenvalues.

Similarly, one can find eigenvalues of the operator $\hat{\mathcal{D}}$

$$\hat{\lambda}_p = \pm \frac{i}{\sqrt{2}} \sqrt{\frac{1}{2} + \frac{K^2}{2}(w + 6) \pm \sqrt{(\frac{K^2}{2}(w - 3) + 2)^2 + 9K^2 - 4}}. \tag{31}$$

From this we calculate the spectral density

$$\hat{\rho}(x) = \lim_{L \rightarrow \infty} \frac{1}{4L^2} \sum_{\lambda} \delta(x - i\hat{\lambda}). \tag{32}$$

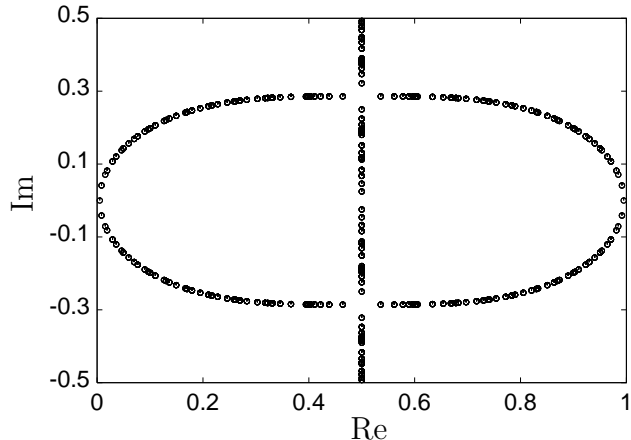


Figure 9: Eigenvalues λ of the Dirac–Wilson operator on a regular triangulation with $L = 50$ and $K = 0.33$.

The spectrum terminates at a small positive value (see fig.10), when K differs from K_{cr} . Only at the $K = K_{cr} = \frac{1}{3}$ it goes directly to zero. In the large L -limit, the two peaks in fig. 10 develop a logarithmic singularity.

For the regular lattice the critical value of the hopping parameter is given by the standard equation $K_{cr} = 1/q$, where q is the number of links emerging from the vertex. In this case $q = 3$. For random lattice this condition is dressed by lattice fluctuations. Although each vertex has coordination $q = 3$, the critical value of the hopping parameter is shifted from $1/3$ to the value given by equation (21). For the regular lattice, the spectrum has an eigenvalue equal exactly zero for the critical hopping parameter. This is not the case for random lattice, where the smallest eigenvalue has a distribution whose center of mass approaches zero only for large N . On the regular lattice, the lowest part of the spectrum does not move when N goes to infinity, but becomes denser. The average distance between the eigenvalues scales like N^{-1/d_H} , with the canonical dimension $d_H = 2$ while on the random lattice, the position of the lowest eigenvalue moves towards zero with N^{-1/d_H} with a dressed exponent $d_H = 2.87(3)$ resulting from the fractal structure of fluctuating geometry.

References

- [1] F. David, Nucl.Phys. **B257** (1985) 45.

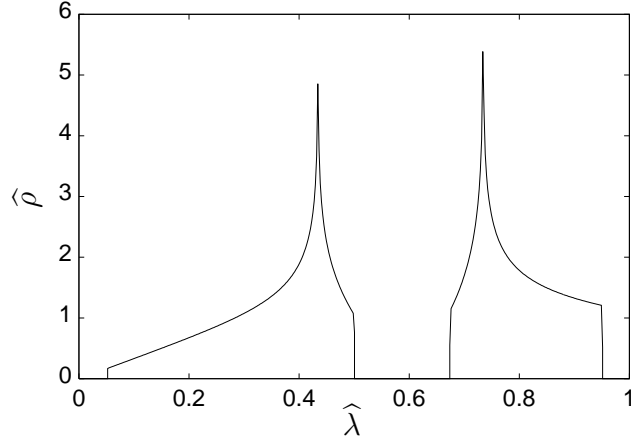


Figure 10: Histograms of eigenvalues of the operator $\hat{\mathcal{D}}$ for $L = 3000$ and $K = 0.3$. At the critical value $K = K_{cr}$ the spectrum goes continuously to zero, while for $K \neq K_{cr}$, like for example for $K = 0.3$ presented in the figure, its low- λ part is cut off at some positive λ_{min} .

- [2] V.A. Kazakov, I.K. Kostov and A.A. Migdal Phys.Lett. **B157** (1985) 295.
- [3] F. David, Simplicial Quantum Gravity and Random Lattices, Les Houches Summer School 1992 Proceedings, hep-th/9303127.
- [4] V.G. Knizhnik, A.M. Polyakov, A.B. Zamolodchikov Mod. Phys. Lett. **A3** (1988) 819.
- [5] F. David, Mod. Phys. Lett **A3** (1988) 509.
- [6] J. Distler and H. Kawai, Nucl. Phys. **B321** (1989) 509.
- [7] M.E. Agishtein, A.A. Migdal, Nucl.Phys. **B385** (1992) 395.
- [8] J. Ambjørn, J. Jurkiewicz Phys.Lett. **B278** (1992) 42.
- [9] P. Bialas, Z. Burda, A. Krzywicki and B. Petersson. Nucl.Phys. **B472** (1996) 293.
- [10] S. Bilke, Z. Burda, A. Krzywicki, B. Petersson, J. Tabaczek, and G. Thorleifsson, Phys.Lett. **B418** (1988) 266.
- [11] H.-C. Ren, Nucl. Phys. **B301** (1988) 661.
- [12] M.A. Bershadsky and A.A. Migdal, Phys. Lett. **B174**, (1986) 393.

- [13] Z. Burda, J. Jurkiewicz and A. Krzywicki, Phys.Rev.**D60** (1999) 105029.
- [14] V.A. Kazakov, Phys. Lett. **A119** (1986) 140.
- [15] D.V. Boulatov, V.A. Kazakov, Phys.Lett. **186B** (1987) 379.
- [16] Z. Burda and J. Jurkiewicz, Acta Phys. Polon. **B20** (1989) 949.
- [17] K. Wilson, Phys.Rev. **D10** (1974) 2445.
- [18] K. Wilson, in *New phenomena in subnuclear physics*, ed. A. Zichichi, Plenum Press, N.Y. 1977 (Erice, '75).
- [19] T. Eguchi, P. B. Gilkey and A. J. Hanson, Phys. Rept. **66** (1980) 213.
- [20] M.B. Green, J.H. Schwarz and E. Witten, *String theory*, Cambridge University Press 1987.
- [21] G.H. Golub, C.F. Van Loan, Matrix Computations, John Hopkins University Press 1996.
- [22] H. Kawai, N. Kawamoto, T. Mogami, Y. Watabiki, Phys. Lett. **B306** (1993) 19.
- [23] H. Kawai, M. Ninomiya, Nucl.Phys. **B336** (1990) 115.
- [24] S. Catterall, G. Thorleifsson, M. Bowick, V. John, Phys.Lett. **B354** (1995) 58.
- [25] M.L. Mehta, *Random matrices* New York Acad. Press (1991) ,
- [26] J.J.M. Verbaarschot, I. Zahed, Phys. Rev. Lett.**70** (1993) 3852.
- [27] J.J.M. Verbaarschot, T. Wettig, Ann. Rev. Nucl. Part. Sci. **50** (2000) 343.